Experimental and Analytical Study of Exponential Power Excursion in Plate-Type Fuel

EXPERIMENTAL AND ANALYTICAL STUDY OF EXPONENTIAL POWER EXCURSION IN PLATE-TYPE FUEL

Lucia Sargentini, Matteo Bucci*
Commissariat à l'énergie atomique et aux énergies alternatives
CEA/DEN/DANS/DM2S/STMF/LATF
91191 Gif-sur-Yvette Cedex, France
*mbucci@mit.edu

Guanyu Su, Jacopo Buongiorno, Thomas McKrell**
Department of Nuclear Science and Engineering
Massachusetts Institute of Technology
77 Massachusetts Avenue, 02138 Cambridge, MA, USA
**jacopo@mit.edu

ABSTRACT

This paper presents an investigation of transient heat transfer, which may occur in nuclear reactors with plate-type fuel during a reactivity initiated accident. Analytical solutions of the heat transfer equation were developed to describe the behavior of plate-type fuel and the MIT pool boiling facility during exponential power excursions governed by conduction heat transfer. Experimental results for non-boiling transient heat transfer tests are also presented and compared to the analytical solutions. Infrared thermometry was used to measure the temperature on the heater surface. The test matrix included exponential power escalations with periods τ as short as 5 milliseconds and water subcoolings ranging from 0 to 78 K. Heat transfer curves and effective heat transfer coefficients to water were measured. The experimental data confirm that the effective heat transfer coefficient decreases monotonically as $1/\sqrt{\tau}$, as expected from the analytical solutions.

KEYWORDS
Reactivity Initiated Accident (RIA), Transient Conduction, Infrared Thermometry

1. INTRODUCTION

A very rapid extraction of control rods in a nuclear reactor core may cause prompt criticality and an exponential excursion of the thermal power generated within the fuel rods. The heat is transferred from the fuel to the coolant which then starts to boil. The heat generation rate in the fuel can be described as $q'''(t) \propto e^{t/\tau}$, where t is time and τ is the period. The feedbacks caused by the heating of fuel and coolant represent an important insertion of negative reactivity. Depending on the magnitude and time scale of these feedbacks, either a safe conclusion to the accident is rapidly achieved or, in extreme cases, the fuel can melt, the molten material expulsed, fragmented and possibly lead to steam explosion. Therefore, the time delay between the production of the thermal energy within the fuel and its transfer to the coolant is key to determining the outcome of the accident, in particular for experimental reactors using highly enriched fissile fuel like the MITR reactor [1], which has a very low Doppler feedback. In turn, this time delay depends on conduction heat transfer within the fuel, non-boiling heat transfer and eventually transient boiling heat transfer in the coolant.

To prove inherent safety features of pool-type water reactors, integral effect experiments were conducted at the Argonne National Laboratory in 1953 and 1954 using the BORAX-I [2] reactor (highly enriched fuel). Experiments demonstrated the intrinsic stability of the reactor core to step insertion of reactivity, up to 2000 pcm (reactor period of 5 ms). A last destructive test was carried out in 1954. To reach core meltdown, an insertion of 4000 pcm was foreseen, but the reactor core exploded after the insertion of 3300 pcm (reactor period of 2.6 ms). After the BORAX investigations, new experiments were undertaken. The SPERT-I pile was designed and built between 1958 and 1962 to explore power excursion between 2.6 and 8 ms of reactor period in stagnant water [3]. Long power excursion periods (≥6 ms) were first addressed, followed by a series of destructive tests at shorter periods. A first test at 4.2 ms led to fuel plate deformation and localized melting. Then, a destructive test was performed, at 3.2 ms (2200 pcm), leading to a partial melting of the core. In the same period, the SPERT-IV pile was used to investigate forced convection effects [4]. The test matrix only included non-destructive tests (minimum period 7 ms). In France, CEA built and operated (1965-1966) the CABRI pile [5]. Only non-destructive tests (periods larger than 10 ms) were performed.

The key role played by heat transfer in the outcome of the accident was rapidly understood and thus, in parallel with the integral effect experiments, separated effect tests were also carried out after the BORAX-I program. In fact, although integral effect experiments were useful to achieve a better understanding of reactor physics, these could not be adequately instrumented to investigate heat transfer phenomena in depth. Hereafter, the main findings of previous experimental investigations are summarized. Non-boiling heat transfer, boiling inception, fully developed nucleate boiling and critical heat flux (CHF) are addressed in the order.

1.1. Non-boiling heat transfer

Exponential transient conduction experiments were first published in 1957 by Rosenthal [6], who used platinum and aluminum ribbons immerged in stagnant water at different temperatures. He observed that for short periods (smaller than 100 ms), the temperature rise was too fast for natural convection to contribute to heat transfer during the non-boiling phase. The leading heat transfer mechanism was instead conduction, for which Rosenthal proposed an analytic solution.
Soliman and Johnson [7] investigated the role of forced convection in the non-boiling regime on a Deltamax® ribbon (50% nickel, 50% iron). They stated that for short periods, much smaller than the travel time of the fluid in the heated channel, an estimate of average wall temperature rise could be obtained by a one-dimensional transversal conduction model combined with a one-dimension longitudinal advection model.
Johnson [8] reported that for stagnant water or low velocity, a reasonably accurate estimate of the single-phase heat transfer coefficient could be obtained with the analytic solution by Rosenthal [6]. For higher velocities, a steady state forced convection coefficient for turbulent flow should be used instead.
In 1977, Sakurai and Shiotsu [9,10] investigated non-boiling heat transfer with a platinum wire in subcooled pool conditions. They showed that the heat transfer coefficient before the initiation of boiling can be estimated by conduction or, for longer periods (> 1 s), natural convection. Using the same wire heater configuration, Kataoka et al. [11] investigated the effect of forced

convection on the single phase heat transfer coefficient, finding results consistent with those obtained by Johnson et al. [7,8].

1.2. Onset of Nucleate Boiling (ONB)

Rosenthal [6] observed a significant rise in the onset of nucleate boiling temperature with respect to the steady heat transfer tests. This temperature rise was higher for shorter periods and higher subcooling, however, for saturation condition, no major differences were observed with respect to steady boiling.
Johnson [8] observed that boiling inception superheat decreases for increasing period and pressure for both pool boiling and low velocity conditions, whereas for higher velocity, a lower superheat was unexpectedly reported for higher subcoolings.
Sakurai and Shiotsu [9] found that wall heat flux and superheat at boiling inception increase with decreasing period and increasing subcooling. Two kinds of boiling incipience models were developed by extending the formulation of Hsu [12] and Rohsenow [13] to explain this behavior.
In 2000, an extensive review on exponential transient heat transfer was published by Sakurai [14]. He pointed out the difference between highly wetting fluids, water pre-pressurized to flood the cavities, and non-pre-pressurized water. In particular, he argued that even for non-pre-pressurized water, for very short period, boiling inception could be triggered by heterogeneous spontaneous nucleation instead of nucleation in active unflooded cavities. Moreover, contrarily to Rosenthal, he showed that, also for saturation conditions and relatively long periods, the onset of nucleate boiling temperature can be significantly higher than in steady boiling.

1.3. From ONB to CHF

Rosenthal [6] reported that, once boiling had started, for subcooled conditions and relatively long period (larger than 15 ms), the behavior of the system was not appreciably different than steady boiling and thus critical heat flux conditions were not influenced by the power excursion period. He also showed the presence of a temperature overshoot between ONB and the fully developed nucleate boiling regime (FDNB).
As also reported by Rosenthal, no major differences with respect to steady boiling were observed by Johnson [8] for the fully developed nucleate boiling regime for periods of 5 ms or longer.
Hall and Harrison [15] first shed light on the peculiarities of transients with very short periods (lower than 5 ms). They used a high speed video camera to observe that, even for very short periods, the boiling crisis was preceded by nucleation of individual bubbles and that during this phase the heat flux could exceed the critical heat flux for steady conditions by an order of magnitude. A similar behavior was also observed by Tachibana et al. [16] for linear power excursion.
Sakurai and Shiotsu [9,10] confirmed the presence of a large temperature overshoot after boiling inception and pointed out the presence of two different boiling processes. The presence of the overshoot (representing impaired heat transfer) was explained as the result of the time leg of activation of initially flooded cavities for the increasing rate of heat flux [10]. In the quasi-static boiling process (i.e. for relatively long periods), fully developed nucleate boiling is attained shortly after the temperature overshoot. In the *rapid* boiling process, when the power excursion periods is very short, the critical heat flux conditions are instead reached before potential active cavities are fully activated. Contrarily to Rosenthal, critical heat flux was observed to vary as a

function of power excursion period and pressure in pool boiling. In fact, Sakurai found that, for subcooled conditions, these increase as the pressure increases and the period decreases, also for relatively long periods (> 5ms) [10]. For saturation conditions the trend is more complicated. Depending on the pressure, the critical heat flux could increase, then decrease and finally increase again as the power excursion period decreases [14].

Although the previous experimental databases form a highly valuable source of information, it must be remarked that sometimes the conclusions of the different authors are quantitatively and qualitatively in disagreement with each other. For these reasons, CEA and MIT have recently decided to undertake a new experimental program devoted to the study of exponential power excursion in both pool boiling and flow boiling conditions. Periods in the range from 5 ms to 1 s and bulk temperatures from saturation to 75K of subcooling will be addressed at both ambient pressure and pressurized conditions. What makes this study unique is the use of state-of-the-art diagnostics such as infrared (IR) thermometry, high-speed video (HSV) and Particle Image Velocimetry (PIV), which have never been used, at our knowledge, to investigate heat transfer phenomena in exponential power excursion and which can provide considerable insight in the physical phenomena occurring at the boiling surface during such rapid transients.
As the first step of this ongoing research program, this paper focuses on the analysis of the non-boiling regime for short periods (transient conduction) and aims at both improving the understanding of the physical phenomena and validating the experimental capabilities to be deployed in future experiments involving actual boiling heat transfer.
In this paper, the heat transfer characteristics of the selected fuel geometry are investigated analytically in Sec.2. The experimental apparatus is described in Sec.3. Scaling of the actual fuel and the experimental configurations is discussed in Sec.4. The experimental results are presented and discussed in Sec.5.

2. ANALYSIS OF TRANSIENT HEAT TRANSFER IN PLATE-TYPE FUEL

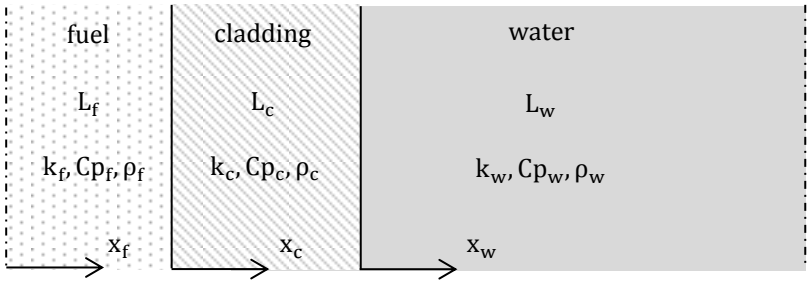

Figure 1 Sketch of plate-type fuel configuration (not to scale).

Conduction heat transfer in plate type fuel during exponential power excursion is investigated using a one-dimensional, symmetric model comprising half of the fuel meat, the cladding and half of the water channel (Figure 1). The governing equations, boundary and initial conditions describing the transient behavior are as follows:

$$\frac{\partial T_f}{\partial t} = a_f \frac{\partial^2 T_f}{\partial x_f^2} + q_0''' e^{\alpha t} \quad \text{(fuel meat)} \qquad (1)$$

$$-k_f \left.\frac{\partial T_f}{\partial x_f}\right|_{x_f=L_f} - k_c \left.\frac{\partial T_c}{\partial x_c}\right|_{x_c=0} = 0 \quad \forall\, t \geq 0 \qquad (2)$$

$$\frac{\partial T_c}{\partial t} = a_c \frac{\partial^2 T_c}{\partial x_c^2} \text{ (cladding)} \quad (3) \qquad -k_c \frac{\partial T_c}{\partial x_c}\Big|_{x_c=L_c} - k_w \frac{\partial T_w}{\partial x_w}\Big|_{x_w=0} = 0 \ \forall\, t \geq 0 \quad (4)$$

$$\frac{\partial T_w}{\partial t} = a_w \frac{\partial^2 T_w}{\partial x_w^2} \text{ (water)} \quad (5) \qquad T_f|_{x_f=L_f} = T_s|_{x_s=0} \ \forall\, t \geq 0 \quad (6)$$

$$-k_w \frac{\partial T_w}{\partial x_w}\Big|_{x_w=L_w} = 0 \ \forall\, t \geq 0 \quad (7) \qquad T_s|_{x_s=L_s} = T_w|_{x_w=0} \ \forall\, t \geq 0 \quad (8)$$

$$-k_f \frac{\partial T_f}{\partial x_f}\Big|_{x_f=0} = 0 \ \forall\, t \geq 0 \quad (9) \qquad T_f|_{t=0} = T_c|_{t=0} = T_w|_{t=0} = T_0 \ \forall\, x_h, x_c, x_w \quad (10)$$

For the short periods of interest to RIA analysis, the time scale of diffusion L^2/a for water is much larger than the power excursion period $\tau = 1/\alpha$. Thus, for the duration of the non-boiling regime, water behaves as an infinite medium ($L_w^2 \gg a_w\, t_{ib}$) and the asymptotic solution of the conduction problem, for $t \gg \tau$ (in general 3τ is large enough), obtained with the Laplace transform method, is given by

$$T_f\,(x_f, t, Fo_w \to 0) = T_0 + \frac{q_0''' e^{\alpha t}}{\rho_f\, Cp_f\, \alpha}\left[1 - \frac{\cosh \dfrac{x_f}{L_f\sqrt{Fo_f}}}{\cosh \dfrac{1}{\sqrt{Fo_f}}}\,\Gamma\right] \quad (11)$$

$$T_c\,(x_c, t, Fo_w \to 0) = T_0 + \frac{q_0''' e^{\alpha t}}{\rho_f\, Cp_f\, \alpha}\left[\cosh \frac{x_c}{L_c\sqrt{Fo_c}} - \left(\cosh \frac{x_c}{L_c\sqrt{Fo_c}} + \sinh \frac{x_c}{L_c\sqrt{Fo_c}}\frac{\mathcal{E}_f}{\mathcal{E}_c}\tanh\frac{1}{\sqrt{Fo_f}}\right)\Gamma\right] \quad (12)$$

$$T_w\,(x_w, t, Fo_w \to 0) = T_0 + \frac{q_0''' e^{\alpha t}}{\rho_f\, Cp_f\, \alpha}\,\exp\left(\frac{-x_w}{\sqrt{a_w\,\tau}}\right)\cosh\frac{1}{\sqrt{Fo_c}}\left[1 - \left(1 + \frac{\mathcal{E}_f}{\mathcal{E}_c}\tanh\frac{1}{\sqrt{Fo_c}}\tanh\frac{1}{\sqrt{Fo_f}}\right)\Gamma\right] \quad (13)$$

with

$$\Gamma = \Gamma(\mathcal{E}_f, \mathcal{E}_c, \mathcal{E}_w, Fo_f, Fo_c) = \frac{\left(\dfrac{\mathcal{E}_w}{\mathcal{E}_c} + \tanh\dfrac{1}{\sqrt{Fo_c}}\right)}{\dfrac{\mathcal{E}_f}{\mathcal{E}_c}\tanh\dfrac{1}{\sqrt{Fo_f}} + \tanh\dfrac{1}{\sqrt{Fo_c}} + \dfrac{\mathcal{E}_w}{\mathcal{E}_c}\left(1 + \dfrac{\mathcal{E}_f}{\mathcal{E}_c}\tanh\dfrac{1}{\sqrt{Fo_c}}\tanh\dfrac{1}{\sqrt{Fo_f}}\right)} \quad (14)$$

where $\mathcal{E} = \sqrt{k\,\rho\,Cp}$ is the thermal effusivity and $Fo = a\,\tau/L^2$ is the asymptotic Fourier number, defined as the ratio between the power excursion period and the time scale of diffusion.

2.1. Heat Fluxes at Interfaces and Energy Transfer Functions

Asymptotic heat fluxes at the fuel-clad and the clad-water interfaces can be thus obtained by differentiation of Eq. 11 and Eq. 13, respectively.

$$q_{fc}''\,(t, Fo_w \to 0) = -k_f \frac{\partial T_f}{\partial\, x_f}\Big|_{x_f=L_f} = q_0''' e^{\alpha t}\,\sqrt{a_f\,\tau}\;\Gamma\;\tanh\frac{1}{\sqrt{Fo_f}} \quad (15)$$

$$q_{cw}''\,(t, Fo_w \to 0) = -k_w \frac{\partial T_w}{\partial\, x_w}\Big|_{x_f=0} = q_0''' e^{\alpha t}\,\sqrt{a_f\,\tau}\,\frac{\mathcal{E}_w}{\mathcal{E}_f}\cosh\frac{1}{\sqrt{Fo_c}}\left[1 - \left(1 + \frac{\mathcal{E}_f}{\mathcal{E}_c}\tanh\frac{1}{\sqrt{Fo_c}}\tanh\frac{1}{\sqrt{Fo_f}}\right)\Gamma\right] \quad (16)$$

Substituting Eq. 16 into Eq. 13, we find:

$$T_w\,(x_w, t, Fo_w \to 0) - T_0 = \frac{q''_{cw}(t)}{\mathcal{E}_w/\sqrt{\tau}}\,\exp\left(\frac{-x_w}{\sqrt{a_w\,\tau}}\right) \tag{17}$$

Eq. 17 correlates the temperature distribution evolution to the wall heat flux during the exponential power excursion.

Energy transfer functions can be defined as the ratio between actual heat flux at the interface and $q'''_0 e^{\alpha t} L_f$, which would be the heat flux required to keep the fuel temperature constant during the power excursion.

$$A_{fc}(Fo_w \to 0) = \frac{q''_{fc}}{q'''_0 e^{\alpha t} L_f} = \Gamma\sqrt{Fo_f}\,\tanh\frac{1}{\sqrt{Fo_f}} \tag{18}$$

$$A_{fw}\,(Fo_w \to 0) = \frac{q''_{cw}}{q'''_0 e^{\alpha t} L_f} = \frac{\mathcal{E}_w}{\mathcal{E}_f}\sqrt{Fo_f}\,\cosh\frac{1}{\sqrt{Fo_c}}\left[1 - \left(1 + \frac{\mathcal{E}_f}{\mathcal{E}_c}\tanh\frac{1}{\sqrt{Fo_c}}\tanh\frac{1}{\sqrt{Fo_f}}\right)\Gamma\right] \tag{19}$$

We remark that, when $\boldsymbol{\tau \ll L_c^2/a_c}$ and $\boldsymbol{\ll L_f^2/a_f}$, Eq. 18 can be reduced to

$$A_{fc,0} = A_{fc}(Fo_w, Fo_c, Fo_f \to 0) = \frac{\mathcal{E}_c}{\mathcal{E}_c + \mathcal{E}_f}\sqrt{Fo_f} \tag{20}$$

The transfer functions are shown in Fig. 2 as a function of period and Fourier numbers, for a sample configuration similar to the SPERT-IV core (U-Al fuel, Al clad). It can be seen that at short periods, only a small part of the heat generated within the fuel is transferred to the cladding and to water. Indeed, the time scale characterizing the production of power is much smaller than the time scale of heat transfer from fuel to clad or from clad to water. In particular, the clad acts like a long-pass filter for the heat, and thus stores most of the energy received from the fuel, if the period is very small.

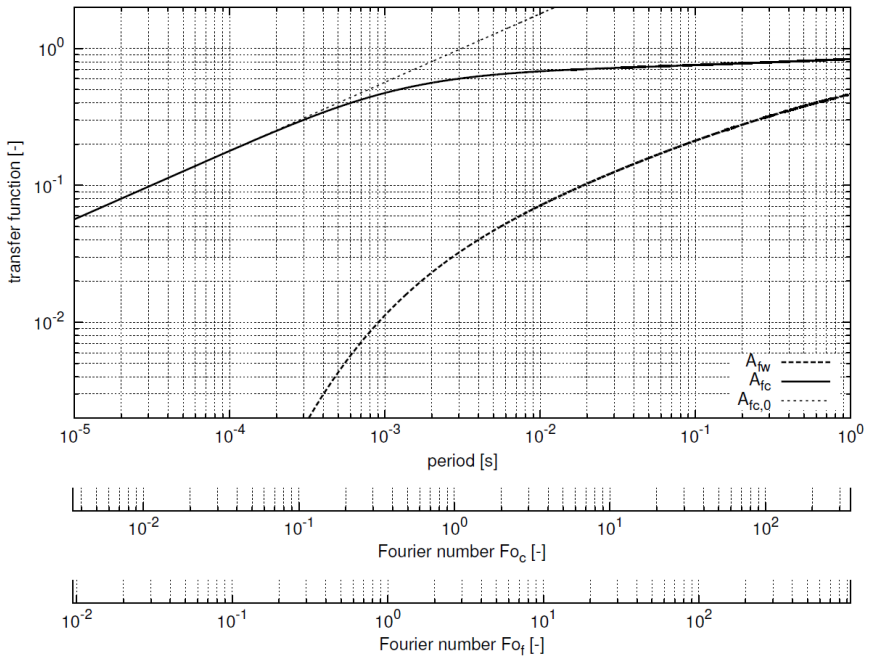

Figure 2 Energy transfer functions in a typical plate-type fuel configuration

2.2. Heat Transfer Coefficient and Thermal Boundary Layer Thickness

Since during the non-boiling phase of the transient, the water channel can be considered as a semi-infinite wall with bulk temperature equal to the initial temperature, we can define the effective transient conduction heat transfer coefficient in water as

$$h_w^{cond} = \frac{q''_{cw}\,(t, Fo_w \to 0)}{T_w\,(x_w = 0, t, Fo_w \to 0) - T_0} = \frac{\mathcal{E}_w}{\sqrt{\tau}} \tag{21}$$

which only depends on the water properties and power excursion period. In asymptotic conditions, the relationship between the wall heat flux, wall temperature, subcooling and wall superheat is therefore

$$q''_{cw} = \frac{\mathcal{E}_w}{\sqrt{\tau}} . (T_{wall} - T_0) = \frac{\mathcal{E}_w}{\sqrt{\tau}} . (T_{wall} - T_{sat} + T_{sat} - T_0) = \frac{\mathcal{E}_w}{\sqrt{\tau}} . (DT_{sat} + DT_{sub}) \tag{22}$$

It is worth mentioning that, even if the heat transfer coefficient increases with a decrease in the power excursion period, the overall effectiveness of heat transfer is impaired, since a smaller fraction of energy is transferred to water (see Fig. 2 and Eq. 19).
Let us define the water thermal boundary layer as the thickness δ_T across which 99% of the temperature variation occurs. It can easily be shown (from Eq. 13) that in our case δ_T is given by:

$$\delta_T = 2 \ln 10 \sqrt{a_w \tau} \tag{23}$$

This equation suggests that, due to the exponential character of the wall heat flux, asymptotic temperature profiles follow a self-similar evolution and the thermal boundary layer thickness only depends on physical properties and power excursion period, but not time. Since the thermal diffusivity of water is very small, the penetration of heat is limited to a very thin layer in the vicinity of the wall, proportional to $\sqrt{a_w \tau}$.

3. DESCRIPTION OF POOL BOILING FACILITY AND EQUIPMENT

The MIT pool boiling facility (PBF) has been used for the present investigation on transient conduction heat transfer. This facility (see Fig. 3) consists of a boiling cell with a specially designed heater, Infrared (IR) thermometry and high-speed video (HSV) with Particle Image Velocimetry (PIV) capabilities. For the scope of the present investigation, only the IR camera was needed.

3.1. Boiling Cell

The boiling cell features a concentric-double-cylinder structure: boiling of degassed deionized (DI) water takes place in the inner cell, while the outer enclosure functions as an isothermal bath. The temperature (and thus the degree of subcooling) of the water in the inner cell is controlled by circulating a temperature-controlled fluid through the isothermal bath. The heater unit sits near the bottom of the cell and accommodates the heater (in red). There are four glass windows spaced equally at 90° around the outer surface of the boiling cell. Two adjacent windows are for the laser illumination and PIV imaging, respectively. A reflux condenser is installed through a hole in the center of the inner cell cover to maintain pressure and prevent reduction of water inventory in the boiling cell. Thermocouples are inserted into the inner cell and the isothermal

bath, to monitor the bulk temperatures of the fluids. All the metal parts are made of stainless steel grade 316, to minimize corrosion. The pool boiling facility is typically operated with water at atmospheric pressure.

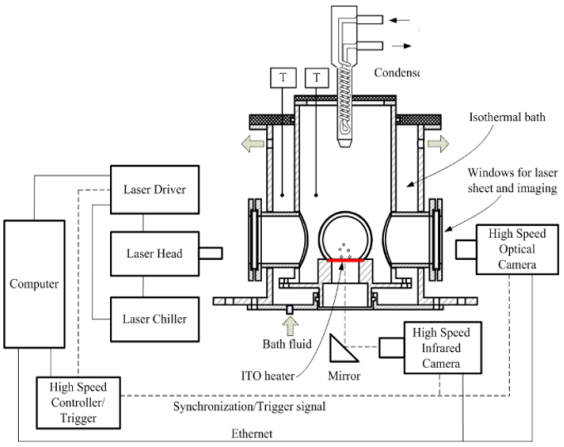

Figure 3 Schematic of the pool boiling facility

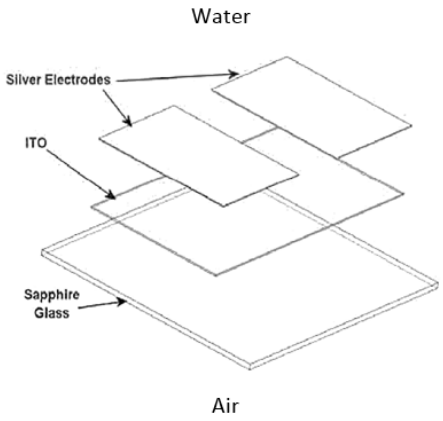

Figure 4 Sapphire heater

3.2. Heater

The heater (see Fig. 4) used for this investigation consists of a thin film of ITO layer (1cm x 2cm, 0.7 micron thick) deposited on a square sapphire substrate (250 microns thick, 5 cm square) with high IR transmissivity. Borosilicate heaters have also been used for tests at 5 and 10 ms of power excursion period and 78 K of subcooling. Two silver pads are attached to the ITO to conduct the electric current that is used to heat the wetted ITO. Silver pads and electrical connections are covered with a protection paint to avoid electrochemical reactions with water. The heater is sealed to the metallic frame with a sticky inert silicon gasket and mechanical clamps.

3.3. IR Camera and IR Thermometry

An IRC800 high-speed infrared camera is used to record the temperature distribution on the heater surface. The sensor of the IR camera captures mid-IR (in the 3-5μm wavelength range) radiation from the ITO heater surface, which is reflected to the sensor of the IR camera through a gold coated mirror. The camera sensor detects the IR radiation intensity and outputs the signal as pixel counts. The conversion from counts to temperature requires multipoint calibration of counts with temperature and the solution of an inverse problem involving thermal conduction and radiation (see Appendix A). A 100mm germanium lens (f/2.3) with a 3/4" extension ring is used. The IR camera has a maximum resolution of 640 x 512 pixels. However, in these experiments, only a small window is needed for imaging the whole ITO heater surface, allowing for a higher frame rate of 4000 fps with an integration time of 0.1 ms. The spatial resolution is approximately 100 microns and the maximum temperature accuracy is 0.5 K.

3.4. High Speed DC Power Supply

A Chroma 62050P-100-100 DC power supply is used to output the electrical power to the heater. The maximum output power is 5kW, with maximum current and voltage of 100A and 100V respectively. The maximum voltage and current slew rates are 10V/ms and 2A/ms, which enable exponential power excursions with periods as small as 5ms. A function generator drives the DC power supply to realize the desired power output. To verify the waveform sent by the power supply, voltage and current outputs are acquired by the data acquisition system with a sampling rate of 10 kHz.

3.5. Synchronizing DC Power Supply, HSV, IR Thermometry and PIV

Synchronization of DC power supply, IR camera and, if needed, HSV camera is obtained via function generators and appropriate triggers as shown in Figure 3. After the function generators receive the same trigger signal, they output different waveforms to the different components, i.e. a square wave for camera and laser synchronization (4000 Hz) and an exponential curve for the DC power supply. The signal that triggers the two cameras is also recorded by the data acquisition system and compared to the power supply output voltage to check their synchronization.

4. ANALYSIS OF TRANSIENT HEAT TRANSFER IN THE HEATER

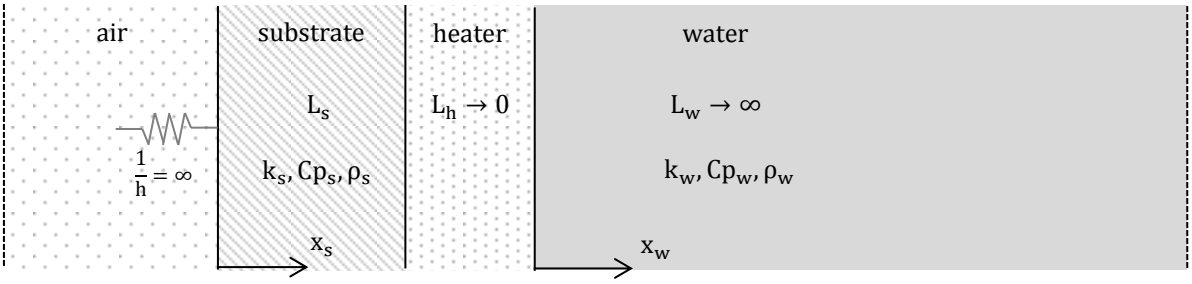

Figure 5 Sketch of the heater configuration (not to scale).

Due to the large aspect ratio between lateral scales (1cm x 2cm) and thickness (250 microns), the system is modeled as one-dimensional conduction heat transfer in the substrate, heater and a semi-infinite water layer (see Fig. 5). The ITO layer is very thin (700 nm) and both its thermal resistance and its thermal capacity are negligible. Therefore, the ITO is modeled as a planar surface energy source given by $q''_{h0}e^{\alpha t}$. The thermal resistance between the substrate and air is very high compared to conduction heat transfer in the substrate and thus the air/substrate interface is assumed to be adiabatic. The equations governing the system, together with the appropriate initial and boundary conditions are:

$$\frac{\partial T_s}{\partial t} = a_s \frac{\partial^2 T_s}{\partial x_s^2} \text{ (substrate)} \qquad (24)$$

$$k_s \frac{\partial T_s}{\partial x_s}\Big|_{x_s=L_s} - k_w \frac{\partial T_w}{\partial x_w}\Big|_{x_w=0} = q''_{h0}e^{\alpha t} \quad \forall\, t \geq 0 \qquad (25)$$

$$\frac{\partial T_w}{\partial t} = a_w \frac{\partial^2 T_w}{\partial x_w^2} \text{ (water)} \qquad (26)$$

$$T_s|_{x_s=L_s} = T_w|_{x_w=0} \quad \forall\, t \geq 0 \qquad (27)$$

$$-k_s \left.\frac{\partial T_s}{\partial x_s}\right|_{x_s=0} = 0 \quad \forall\, t \geq 0 \tag{28}$$

$$T_s|_{t=0} = T_w|_{t=0} = T_0 \quad \forall\, x_s, x_w \tag{29}$$

$$T_w|_{x_w=\infty} = T_0 \quad \forall\, t \geq 0 \tag{30}$$

The asymptotic solution of the conduction problem for the non-boiling regime is

$$T_s\,(x_s, t) = T_0 + \frac{q''_{h0} e^{\alpha t}}{\sqrt{\alpha}} \left[\cosh \frac{x_s}{L_s \sqrt{Fo_s}} \Big/ \cosh \frac{1}{\sqrt{Fo_s}}\right] \Big/ \left[\mathcal{E}_s \tanh \frac{1}{\sqrt{Fo_s}} + \mathcal{E}_w\right] \tag{31}$$

$$T_w\,(x_w, t) = T_0 + \frac{q''_{h0} e^{\alpha t}}{\sqrt{\alpha}} \left[\exp\left(\frac{-x_w}{\sqrt{a_w\,\tau}}\right)\right] \Big/ \left[\mathcal{E}_s \tanh \frac{1}{\sqrt{Fo_s}} + \mathcal{E}_w\right] \tag{32}$$

and the heat fluxes at the interface with ITO are thus given by

$$q''_{hs}\,(t) = k_s \left.\frac{\partial T_s}{\partial\, x_s}\right|_{x_s=L_s} = q''_{h0} e^{\alpha t} \;\; \mathcal{E}_s \tanh \frac{1}{\sqrt{Fo_s}} \Big/ \left[\mathcal{E}_s \tanh \frac{1}{\sqrt{Fo_s}} + \mathcal{E}_w\right] \tag{33}$$

$$q''_{hw}\,(t) = -k_w \left.\frac{\partial T_w}{\partial\, x_w}\right|_{x_f=0} = q''_{h0} e^{\alpha t} \;\; \mathcal{E}_w \Big/ \left[\mathcal{E}_s \tanh \frac{1}{\sqrt{Fo_s}} + \mathcal{E}_w\right] \tag{34}$$

It can easily be seen that the correlation between temperature profile evolution and the wall heat flux is identical to the one we found for the fuel plate (see Eq. 17)

$$T_w\,(x_w, t) - T_0 = \frac{q''_{hw}(t)}{\mathcal{E}_w/\sqrt{\tau}} \exp\left(\frac{-x_w}{\sqrt{a_w\,\tau}}\right) \tag{35}$$

and therefore for a given period and a given bulk temperature (physical properties), the asymptotic heat transfer coefficient and the boundary layer thickness are the same for the two configurations. To achieve the same temperature profile history, the source term q''_{h0} should be adjusted to have $q''_{hw} = q''_{cw}$, that happens when

$$q''_{h0} = q'''_0 \sqrt{a_f\,\tau}\, \frac{\mathcal{E}_s \tanh \frac{1}{\sqrt{Fo_s}} + \mathcal{E}_w}{\mathcal{E}_f} \cosh \frac{1}{\sqrt{Fo_c}} \left[1 - \left(1 + \frac{\mathcal{E}_f}{\mathcal{E}_c} \tanh \frac{1}{\sqrt{Fo_c}} \tanh \frac{1}{\sqrt{Fo_f}}\right) \Gamma\right] \tag{36}$$

5. ANALYSIS OF EXPERIMENTAL RESULTS

Transient conduction experiments have been carried out in the pool boiling facility using heaters on both sapphire and borosilicate substrates. Three subcoolings have been investigated: 0, 36 and 78 K. Power excursion periods have been varied between 5 and 100 ms. The results of this experimental investigation are summarized in Fig. 6 through Fig. 10. First, note the near-perfect agreement between analytical and experimental curves for all the cases tested.

In Fig. 6 through Fig. 9, the experimental heat transfer curves for the three subcoolings are shown, together with asymptotic transient conduction curves, as predicted by Eq. 22. In Fig. 6 through Fig. 8, the dependence on the power excursion period is shown for a fixed subcooling whereas Fig. 9 shows the dependence on subcooling for a fixed power excursion period. The curves are plotted as a function of the wall superheat DT_{sat}, and the water properties are taken at saturation temperature. Experiments were intentionally stopped before boiling could start and thus wall temperatures are limited to about 110 °C. It can be seen that, even for tests with longer periods (50, 70 and 100 ms) at saturation conditions, the heat transfer curves all merge into an

asymptotic conduction curve before the end of the non-boiling transient. As expected, for smaller periods (Fig. 6 through Fig. 8) and larger subcooling (Fig. 9), the heat flux that can be transferred to water for a given wall temperature is higher. In particular, it is worth mentioning that for very small periods (20 to 5 ms) and large subcooling (78 K) the conduction heat flux at the wall can exceed values (1 MW/m^2) that in steady state tests typically result in boiling and even critical heat flux.

Fig. 10 shows the experimental effective heat transfer coefficients as a function of period, for the three subcoolings, together with the asymptotic conduction heat transfer coefficient, as predicted by Eq. 21. Five runs were performed for each experimental point. Therefore, the datapoints reported in Fig. 10 are the time-averages of the instantaneous heat transfer coefficient values for these 5 runs, over the temperature range shown in Fig. 6 through Fig. 9 (error bars corresponds to experimental repeatability expressed as ±2σ). As expected from the analytical solutions, the heat transfer coefficient depends on the power excursion period (it is proportional to $1/\sqrt{\tau}$), but not on the subcooling.

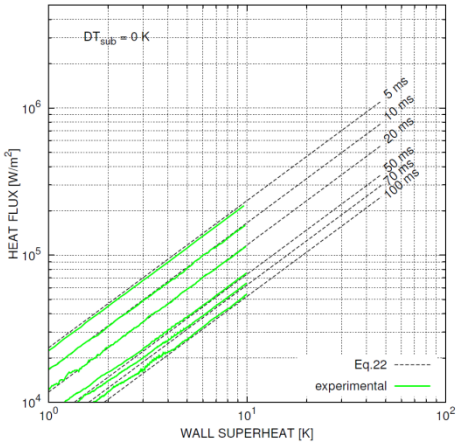

Figure 6 Heat transfer curves (DT_{sub} = 0 K)

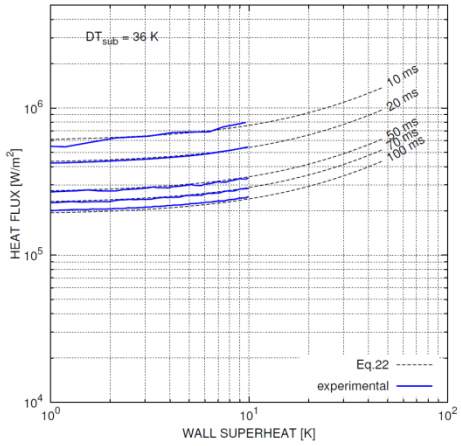

Figure 7 Heat transfer curves (DT_{sub} = 36 K)

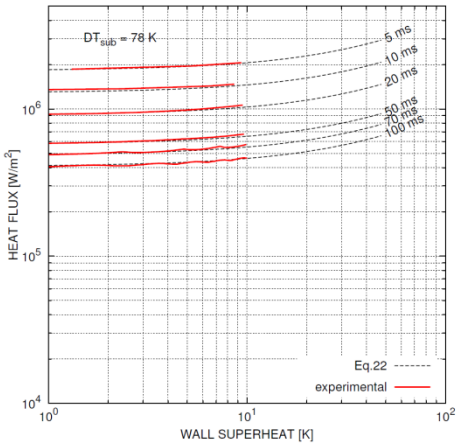

Figure 8 Heat transfer curves (DT_{sub} = 78 K)

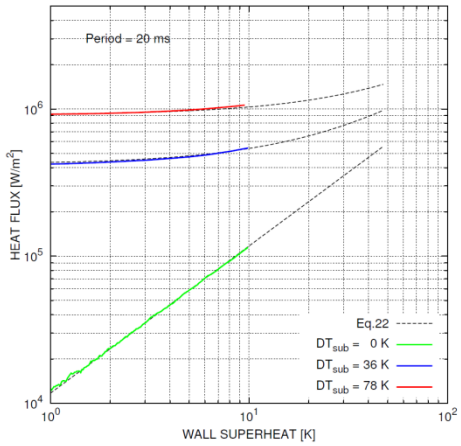

Figure 9 Heat transfer curves (τ = 20 ms)

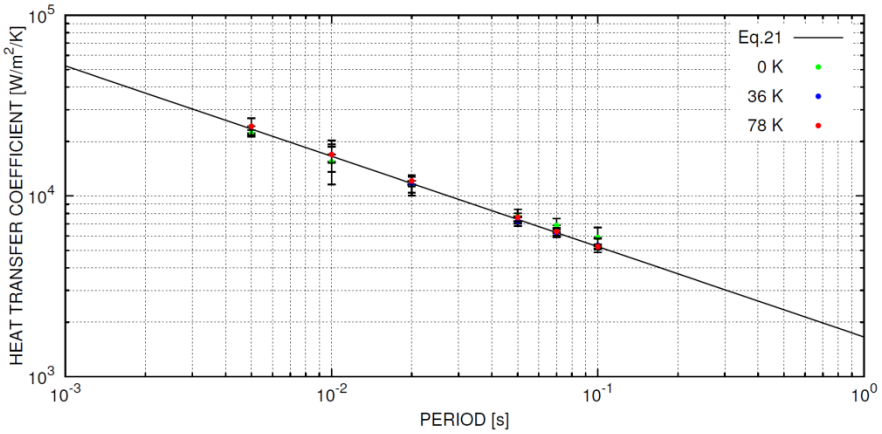

Figure 10 Single-phase heat transfer coefficients

6. CONCLUSIONS

A theoretical analysis of exponential power excursion governed by conduction heat transfer has been performed for plate-type fuel configurations, typical of certain test and research reactors. Single phase energy transfer from the fuel to the coolant has been quantified as a function of geometry, material properties and period of the exponential power excursion. The heat transfer delay associated with the presence of the cladding has been quantified, revealing that the cladding acts like a long-pass filter and stores most of the energy released by the fuel when the power excursion period is very short (<10 ms). Transient heat transfer in the coolant has been also analyzed. The analysis has confirmed that during exponential power excursions governed by conduction, the asymptotic heat transfer coefficient between the cladding and the coolant is proportional to the thermal effusivity of water and increases as the period decrease, as $1/\sqrt{\tau}$.
Then, such exponential power excursions have been investigated experimentally in the MIT pool boiling facility, adopting infrared thermometry diagnostics to determine wall temperature and heat flux during the transient. These investigations have fully confirmed the accuracy and trends of the results of the theoretical analysis and have proved the capability of the experimental setup to investigate these phenomena, which is promising in view of future investigations involving transient boiling heat transfer. It is also noteworthy that, due to the exponential nature of the transient, for large subcoolings and short periods, the conductive heat flux at the wall can exceed values that usually lead to boiling and critical heat flux in steady conditions.

ACKNOWLEDGMENTS

This research project was sponsored by CEA through contract 021439-001.

REFERENCES

1. http://web.mit.edu/nrl/www/reactor/reactor.htm
2. J.R. Dietrich, D.C. Layman, *Transient and Steady State Characteristics of a Boiling Reactor: the BORAX experiments*, U.S. Atomic Energy Commission Report AECD-3840 (1954).
3. F. Schroeder, S. G. Forbes, W. E. Nyer, F. L. Bentzen, G. O. Bright, "Experimental Study of Transient Behavior in a Subcooled Water-Moderated Reactor," *Nuclear Science and Engineering*, **2**, pp.97-115 (1957).

4. J.G. Crocker, L.A. Stephan, *Reactor power Excursion Tests in the SPERT-IV Facility*, U.S. Atomic Energy Commission Report IDO-17000 (1954).
5. J. Papin, M. Balourdet, F. Lemoine, "French Studies on High-Burnup Fuel Transient Behavior under RIA Conditions," *Nuclear Safety*, **37**, pp.289-327 (1996).
6. M.W. Rosenthal, "An Experimental Study of Transient Boiling," *Nuclear Science and Engineering*, **2**, pp.640-656 (1957).
7. M. Soliman, H. A. Johnson, "Transient Heat Transfer for Forced Convection over a Flat Plate of Appreciable Thermal Capacity and Containing an Exponential Time-Dependent Heat Source," *International Journal of Heat and Mass Transfer*, **11**, pp.27-38 (1968).
8. H.A. Johnson, "Transient Boiling Heat Transfer to Water," *International Journal of Heat and Mass Transfer*, **14**, pp.67-82 (1971).
9. A. Sakurai, M. Shiotsu, "Transient Pool Boiling Heat Transfer. Part 1: Incipient Boiling Superheat," *Journal of Heat Transfer*, **99**, pp.547-553 (1977).
10. A. Sakurai, M. Shiotsu, "Transient Pool Boiling Heat Transfer. Part 2: Boiling Heat Transfer and Burnout," *Journal of Heat Transfer*, **99**, pp.554-560 (1977).
11. I. Kataoka, A. Serizawa, A. Sakurai, "Transient Boiling Heat Transfer under Forced Convection," *International Journal of Heat and Mass Transfer*, **26**, pp.583-595 (1983).
12. Y. Y. Hsu, "On the Size Range of Active Nucleation Cavities on a Heating Surface," *Journal of Heat Transfer*, **14**, pp.67-82 (1971).
13. W.M. Rohsenow, "Nucleation in Boiling Heat Transfer," ASME Paper 70-HT-18, *ASME Symposium*, Detroit, (1970).
14. A. Sakurai, "Mechanism of Transition to Film Boiling at CHF in subcooled and Pressurized Liquids due to Steady and Increasing Heat Inputs," Nuclear Engineering and Design, **197**, pp.301-356 (2000).
15. W.B. Hall, W.C. Harrison, "Transient Boiling of Water at Atmospheric Pressure," *International Heat Transfer Conference*, Instit. Mech. Eng., Chicago, Illinois, (1966).
16. F. Tachibana, M. Akiyama, H. Kawamura, "Heat Transfer and Critical Heat Flux in Transient Boiling," *Journal of Nuclear Science and Technology*, **5**, pp.117-126 (1968).

APPENDIX A. COUPLED CONDUCTION/RADIATION MODEL

A.1. Conduction Model

The heat transfer equation is discretized with a finite volume scheme in the physical domain sketched in Fig. 5. For the transient conduction phase, a simple 1D model can be adopted. The adiabatic boundary condition is applied at the interface between the substrate and air. A constant subcooling temperature is imposed at the right boundary of the water layer, and the water layer thickness is chosen sufficiently high not to affect the results. The temperature of the ITO is fixed according to the photon counts recorded by the infrared camera, as described below (Sec. A.4). The heat conduction problems in the substrate and in the coolant are thus solved separately. Once the converged solution is achieved for a prescribed ITO temperature, heat fluxes at the interface substrate/ITO and ITO/water can be inferred from the temperature gradients.

A.2. Radiation Model

Photons are emitted by the ITO layer and by the substrate. Water emissions are completely shielded by the ITO layer, which is opaque in the range 3 to 5 microns used in our investigations.

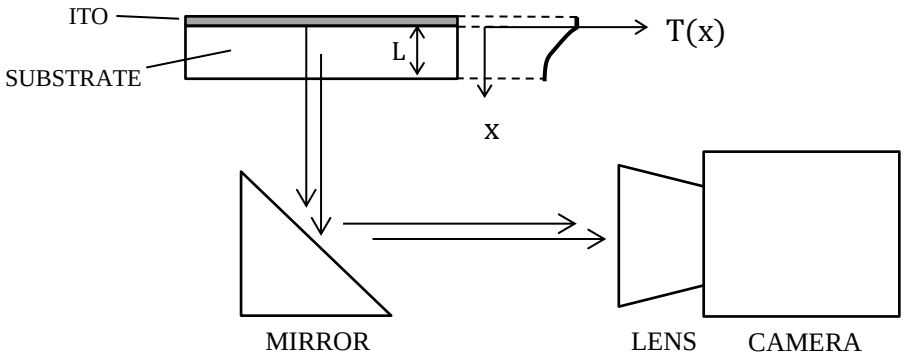

Figure 11 Sketch of the optical setup

The spectral hemispherical photon flux per wavelength emitted by a black body is

$$N_{p\lambda} = N_{p\lambda}(T,\lambda) = \frac{2\,\pi\,c}{\lambda^4\left(e^{\frac{C_2}{\lambda T}}-1\right)} \tag{37}$$

Since ITO is thick enough to be considered opaque, the spectral photon flux emitted at the interface between the ITO and the substrate is

$$N_{p\lambda,T_h}.\left(1-\rho_{\lambda,hs}\right) \tag{38}$$

where $\rho_{\lambda,hs}$ is the spectral reflection coefficient at the interface ITO/substrate and T_h is temperature of the ITO, which can be considered constant through its thickness. Then, to obtain the effective photon flux emitted by the ITO, one must take into account multiple reflections at the ITO/substrate and substrate/air interfaces and absorption within the substrate:

$$N_{p\lambda}^{ito} = N_{p\lambda,T_h}\left(1-\rho_{\lambda,hs}\right)\tau_{\lambda,s}\left(1-\rho_{\lambda,sa}\right)\sum_{n=0}^{\infty}\left(\rho_{\lambda,hs}\,\rho_{\lambda,sa}\,\tau_{\lambda,s}^2\right)^n = N_{p\lambda,T_h}\frac{\left(1-\rho_{\lambda,hs}\right)\tau_{\lambda,s}\left(1-\rho_{\lambda,sa}\right)}{1-\rho_{\lambda,hs}\,\rho_{\lambda,sa}\,\tau_{\lambda,s}^2} = N_{p\lambda,T_h}\tau_{\lambda,app} \tag{39}$$

A substrate layer of thickness dx emits a photons flux equal to $\alpha_\lambda N_{p\lambda,T(x)} dx$ in two directions. Half of the flux is emitted forward, towards the camera, half is emitted backward, towards the ITO heater. In the first case, the spectral photons flux reaching the substrate/air interface is

$$N_{p\lambda}^{s,+} = \int_0^L \alpha_\lambda \, N_{p\lambda,T(x)} \exp\left(-\alpha_\lambda (L-x)\right) dx \tag{40}$$

In the second case, the photons flux reaching the ITO/substrate interface is instead given by

$$N_{p\lambda}^{s,-} = \int_0^L \alpha_\lambda \, N_{p\lambda,T(x)} \exp(-\alpha_\lambda x) \, dx \tag{41}$$

Part of this flux is reflected back at the substrate/ITO interface and crosses the substrate to reach the substrate/air interface. At the substrate/air interface, the two light beams can be transmitted or reflected. Once multiple reflections and absorptions are accounted for, the effective spectral photons flux crossing the substrate/air interface is

$$N_{p\lambda}^{s} = \frac{N_{p\lambda,T(x)}^{s,-} \, \rho_{\lambda,hs} \, \tau_{\lambda,s} \left(1-\rho_{\lambda,sa}\right) + N_{p\lambda,T(x)}^{s,+} \left(1-\rho_{\lambda,sa}\right)}{1 - \rho_{\lambda,hs} \, \rho_{\lambda,sa} \, \tau_{\lambda,s}^2} = N_{p\lambda,T(x)}^{s,-} \epsilon_{\lambda,app}^{-} + N_{p\lambda,T(x)}^{s,+} \epsilon_{\lambda,app}^{+} \tag{42}$$

Part of the signal reaching the IR camera is due to reflection of the background emission at the ITO/substrate and substrate/air interfaces. The atmosphere emits like a blackbody, and the spectral photons flux reflected by the heater is given by

$$N_{p\lambda}^{a} = N_{p\lambda,T_a} \left(\rho_{\lambda,sa} + \frac{\rho_{\lambda,hs} \, \tau_{\lambda,s}^2 \left(1-\rho_{\lambda,sa}\right)^2}{1 - \rho_{\lambda,hs} \, \rho_{\lambda,sa} \, \tau_{\lambda,s}^2} \right) = N_{p\lambda,T_a} \, \rho_{\lambda,app} \tag{43}$$

The spectral overall photons flux emitted at the substrate/air interface is thus given by

$$N_{p\lambda} = N_{p\lambda,T_h} \tau_{\lambda,app} + N_{p\lambda,T_a} \rho_{\lambda,app} + N_{p\lambda,T(x)}^{s,-} \epsilon_{\lambda,app}^{-} + N_{p\lambda,T(x)}^{s,+} \epsilon_{\lambda,app}^{+} \tag{44}$$

The spectral flux can be integrated over the range of interest (3 to 5 micrometers) to obtain the effective photons flux

$$N_p = \int_{\lambda_1}^{\lambda_2} N_{p\lambda} d\lambda = \int_{\lambda_1}^{\lambda_2} N_{p\lambda,T_h} \tau_{\lambda,app} d\lambda + \int_{\lambda_1}^{\lambda_2} N_{p\lambda,T_a} \rho_{\lambda,app} d\lambda + \int_{\lambda_1}^{\lambda_2} N_{p\lambda,T(x)}^{s,-} \epsilon_{\lambda,app}^{-} d\lambda + \int_{\lambda_1}^{\lambda_2} N_{p\lambda,T(x)}^{s,+} \epsilon_{\lambda,app}^{+} d\lambda \tag{45}$$

Finally, only a fraction of the photons emitted by the heater is directed towards the lens and can reach the camera sensor. The final flux depends essentially on the lens focal number n_f and can be estimated by

$$\frac{N_p}{4 \, n_f^2} \, \tau_{os} \tag{46}$$

where the transmission efficiency of the optical setup τ_{os} (mirror and lens) is also accounted for.

A.3. Conversion from camera counts to photons

An IRC800 high-speed infrared camera with an InSb photon detector is used. Each pixel of the InSb sensor has a well of 7 million electrons. Every time a photon hits the pixel, one electron is moved from the valence to the conduction band and generates a current, which is the signal measured as camera counts. The quantum efficiency of the sensor, QE, which is determined by the photon/electron conversion efficiency, as well as reflection on the surface of the sensor, must be also taken into account.

To convert camera counts to photons, the contribution of noise must be cancelled. This is given by empty well counts when the integration time int_time is zero (approximately 300 counts) and

dark current (9570 counts/second), whose noise is proportional to the integration time (0.1 ms). The effective photons flux measured by the camera is thus given by

$$N_p^{IRC} = \frac{\text{ncounts} - (\text{ewell} + \text{darkcurrent} \cdot \text{int\_time})}{\text{int\_time}} \cdot \frac{7.\text{E} + 6}{(\text{fwell} - \text{ewell})} \cdot \frac{1}{\text{QE}} \tag{47}$$

where fwell is the counts when the signal is saturated (approximately 16000 counts).

A.4. Conduction/Radiation Coupling

At a given time step, the photon counts from the IR camera are obtained. Then a guess of the heater temperature is made based on the temperature distribution at the previous time step. The temperature distribution through the substrate is solved by the heat conduction code. The emission from the ITO and the substrate are calculated from the temperature distribution within the substrate and then converted to photon counts (inversion of Eq.47). Then the photon counts obtained by the conduction/radiation model are compared to the camera reading. If the difference of photon counts is less than a prescribed tolerable error, the guessed temperature of ITO heater is accepted and the code is moved to the next time step, otherwise, the code keeps iterating with another guess of the ITO temperature as boundary condition. The flow chart of the code is shown in Fig. 12.

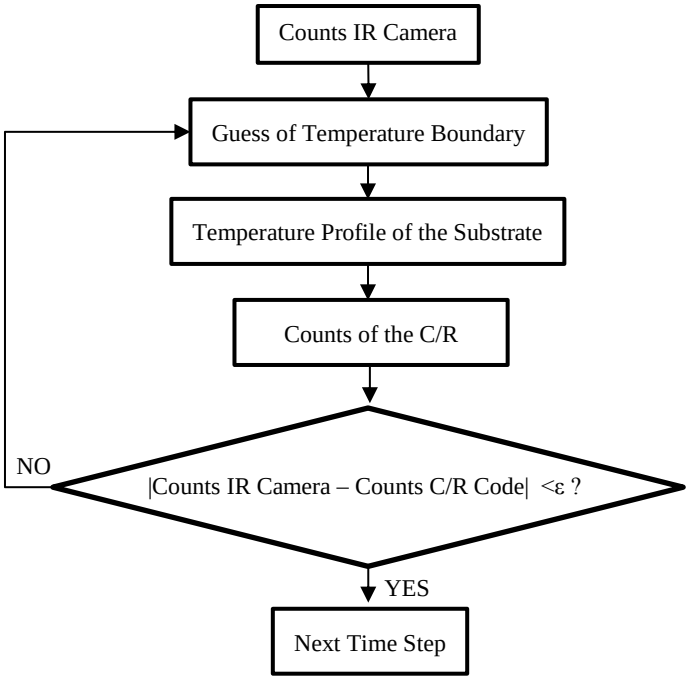

Figure 12 Flow Chart for Conduction/Radiation Coupling

It should be noted that verification of the conduction/radiation coupling is required before every experimental campaign (every heater and camera position). Fine tuning of the quantum efficiency and the transmissivity of lens and mirror is also necessary to reduce the error on the measured photons flux. This is normally achieved by steady-state calibration, to be run before every transient experiment.

LIST OF SYMBOLS

Latin letters

a	Thermal diffusivity	$[m^2/s]$
A	Transfer function	$[-]$
Cp	Specific heat	$[J/kgK]$
C_2	$=1.439x10^{-2}$ (appendix)	$[mK]$
c	Speed of light	$[m/s]$
DT	Temperature difference	[K]
Fo	Fourier number	$[-]$
h	Heat transfer coefficient	$[W/m^2K]$
k	Thermal conductivity	$[W/mK]$
L	Thickness	[m]
N_p	Photons flux (appendix)	$[phot/m^2s\ m]$
n_f	Focal number (appendix)	$[-]$
q''	Heat flux	$[W/m^2]$
q'''	Energy source	$[W/m^3]$
QE	Quantum efficiency (appendix)	$[-]$
t	Time	[s]
T	Temperature	[K]
x	Spatial coordinate	[m]

Greek letters

α	$1/\tau$	$[1/s]$
α	Absorption coefficient (appendix)	$[1/m]$
Γ	Function defined by Eq. 14	$[-]$
δ_T	Thermal boundary layer thickness	[m]
$\mathcal{E}$	Thermal Effusivity	$[W\sqrt{s}/m^2K]$
ϵ	Apparent emissivity (appendix)	$[-]$
c	Wavelength	[m]
ρ	Density	$[kg/m^3]$
ρ	Reflectivity (appendix)	$[-]$
τ	Exponential period	[s]
τ	Transmissivity (appendix)	$[-]$

Subscripts

0	Initial
0	Asymptotic ($\tau \rightarrow 0$)
app	Apparent (appendix)
c	Cladding
f	Fuel
ib	Boiling Inception
h	Heater (ITO)
os	Optical Setup
s	Substrate
sat	Superheat
sub	Subcooling
w	Water

Index

a	Atmosphere
cond	Conduction
IRC	Infrared camera
ITO	Indium-Tin-Oxide
s	Substrate